ELASTIC SEISMIC ENVELOPE INVERSION

JINGRUI LUO[1,2], RU-SHAN WU[2] and JINGHUAI GAO[3]

[1] *School of Automation and Information Engineering, Xi'an University of Technology, Xi'an 710048, P.R. China. bluebirdjr@126.com*
[2] *Modeling and Imaging Laboratory, Earth & Planetary Sciences, Univ. of California, Santa Cruz, CA 95064, U.S.A. rwu@ucsc.edu*
[3] *National Engineering Laboratory on Offshore Exploration, Xi'an Jiaotong University, Xi'an 710049, P.R. China*

(Received May 20, 2015; accepted November 5, 2015)

ABSTRACT

Luo, J., Wu, R.-S. and Gao, J., 2016. Elastic seismic envelope inversion. *Journal of Seismic Exploration*, 25: 103-119.

We propose the elastic seismic envelope inversion method, which is an extension of our previous work about the acoustic situation. Seismic full waveform inversion suffers severely from the local minima problem, which comes from the lack of low frequency information in the data. The envelope of the data carries ultra low frequency information and thus can be used to construct the large scale component of the model. We give the method of envelope inversion for the elastic situation where P-wave velocity and S-wave velocity are inverted simultaneously. Numerical examples using the Marmousi II model proved that the combined elastic envelope inversion plus waveform inversion (EI+WI) provides much better results than the conventional elastic full waveform inversion, especially for the case of lacking low frequency information in the seismic data.

KEY WORDS: full waveform inversion, envelope inversion, elastic.

INTRODUCTION

Lally (1883) and Tarantola (1984) first proposed the full waveform inversion method in the acoustic approximation. Later Tarantola (1986) gave the theory for elastic full waveform inversion and showed the choice of parameters for the inversion. Mora (1987, 1988) implemented the elastic inversion using a preconditioned conjugate gradient algorithm and gave the inversion results from synthetic data sets. After that, many authors have investigated the elastic full waveform inversion (Sambridge et al., 1991; Crase et al., 1992; Debski and Tarantola, 1995; Djipéssé and Tarantola, 1999; Sears et al., 2008; Sears et al., 2010). However, as in acoustic situation, in order to get good inversion results, we always need good initial models.

0963-0651/16/$5.00 © 2016 Geophysical Press Ltd.

The difficulty of initial model construction comes from the lack of low frequency information in the seismic data. If we have low frequency information, then a successive inversion from low frequency to high frequency using the time domain multiscale method (Bunks et al., 1995) or the frequency domain method (Pratt, 1999; Pratt and Shipp, 1999; Brenders and Pratt, 2007) will be fine. These methods allow us to first get the long wavelength background from the low frequency signal and then get the details from high frequency signal. However, there is always no low frequency signal existing in the seismic source, and the generation of low frequency signal below 5 Hz is very expensive. Therefore, the important thing is how to get the long wavelength background model without low frequencies.

Several approaches have been proposed to reduce this problem in recent years. Shin and Cha (2008, 2009) developed the Laplace domain and the Laplace-Fourier domain full waveform inversion.

They used the damped signal in their method and can provide a smooth background model for the inversion. Liu et at. (2011) developed the normalized integration method. Biondi and Almomin (2012, 2013, 2014) combined full waveform inversion with wave equation migration velocity analysis and used extended lag in their method. Wang et al. (2012) combined wave equation tomography and full waveform inversion in the misfit function. Warner and Guasch (2014) developed the adaptive waveform inversion method in which the Wiener filter is measured. Wu et al. (2013, 2014) and Luo et al. (2013, 2015) proposed the envelope inversion (EI) method where the envelope of the seismic data is used and which can give a very smooth background model.

The above approaches are mostly developed in the acoustic situation. However, as we all know, the real earth is elastic, so it would be better to perform elastic waveform inversion rather than acoustic. In this paper, we extend our previously proposed envelope inversion method to the elastic situation. We first give the theory of this method where we show the misfit for the elastic envelope inversion and derive the gradient for P-wave velocity and S-wave velocity. Then we use the Marmousi II model to prove the validity of this method. To further test the independence of this method to the source frequency band, we used a low-cut (cut from 5 Hz below) source wavelet for the inversion. Numerical tests showed that the combined inversion elastic EI+WI can provide much more faithful and accurate final results than the conventional elastic FWI.

ELASTIC FULL WAVEFORM INVERSION IN THE TIME DOMAIN

The 2D isotropic elastic wave equation has the following expression,

$$\rho(\partial^2 u^i/\partial t^2) - (\partial \tau^{ij}/\partial x^j) = f^i \quad ,$$
$$\tau^{ij} = M^{ij} + \lambda \delta^{ij} u_{k,k} + \mu(u_{i,j} + u_{j,i}) \quad . \tag{1}$$

Here the Einstein summation convention is used. In the above equation, u^i is the i-th component for the displacement vector, τ^{ij} means the ij component for the stress tensor. λ and μ are the Lamé coefficients, and ρ is the density. f^i is the body force and M^{ij} is the traction. The relationship between P-, S-wave velocity and Lamé coefficients is given by,

$$v_P = \sqrt{[(\lambda + 2\mu)/\rho]} \quad ,$$
$$v_S = \sqrt{(\lambda/\rho)} \quad . \tag{2}$$

The most commonly used least squares misfit function for elastic full waveform inversion in the time domain has the following form,

$$\sigma(\mathbf{m}) = \tfrac{1}{2} \sum_{sr} \sum_{i} \int_0^T [s^i(t) - u^i(t)]^2 dt \quad . \tag{3}$$

where s^i is the i-th component of the synthetic wavefield, u^i is the i-th component of the observed wavefield, and $\mathbf{m}$ is the model parameter. We assume that the density is constant, and consider v_P and v_S as the model parameters. The gradient of the misfit function σ with respect to v_P and v_S can be obtained by

$$\partial\sigma/\partial v_P = \sum_{sr} \sum_{i} \int_0^T [s^i(t) - u^i(t)](\partial s^i/\partial v_P) dt \quad ,$$
$$\partial\sigma/\partial v_S = \sum_{sr} \sum_{i} \int_0^T [s^i(t) - u^i(t)](\partial s^i/\partial v_S) dt \quad . \tag{4}$$

Introduce the Jacobian operator $(\mathbf{J}_P, \mathbf{J}_S)$ and data residual vector η, where

$$\begin{matrix} \mathbf{J}_P = \partial s^i/v_P \\ \mathbf{J}_S = \partial s^i/v_S \end{matrix} \quad , \quad \eta = s^i - u^i \quad . \tag{5}$$

Then eq. (4) can be written in the following form,

$$\begin{matrix} \partial\sigma/\partial v_P = \mathbf{J}_P^T \eta \\ \partial\sigma/\partial v_S = \mathbf{J}_S^T \eta \end{matrix} \quad . \tag{6}$$

The Jacobian ($\mathbf{J}_P$,$\mathbf{J}_S$) is also known as the Fréchet derivative. We can use the backpropagation method to calculate the gradient in eq. (6), which is the zero-lag correlation of the forward propagated source wavefields and the backward propagated residual wavefields (for details see Appendix A).

ELASTIC SEISMIC ENVELOPE INVERSION METHOD

Trace envelope extraction

We start from the introduction of the definition of trace envelope. The envelope of a trace can be extracted by taking the amplitude after the analytical signal transform using the Hilbert transform. Each real signal has a corresponding analytic signal $\tilde{f}(t)$ which can be constructed from the original real signal f(t) and its Hilbert transform $H\{f(t)\}$,

$$\tilde{f}(t) = f(t) + iH\{f(t)\} \quad . \tag{7}$$

The Hilbert transform is defined by

$$H\{f(t)\} = -(1/\lambda)P \int_{-\infty}^{+\infty} [f(\tau)/(t-\tau)]d\tau \quad , \tag{8}$$

where P is the Cauchy principal value.

The envelope of f(t) can then be obtained by

$$e(t) = \sqrt{[f^2(t) + H\{f(t)\}^2]} \quad , \tag{9}$$

From the above we see that we can easily get the envelope of a signal from the Hilbert transform.

Shot gathers

In the following we show the property of the envelope from a shot gather example. Fig. 1(a) shows the data traces from the Marmousi II model. Both the x-component and the z-component of the wavefields are shown. The data was generated using a Ricker wavelet with the dominate frequency of 10 Hz. Fig. 1(b) shows the envelope of the traces in (a). We can see that the envelopes look much smoother than the original traces. Then we analyze the spectra of the original traces [Fig. 1(c)] and the trace envelopes [Fig. 1(d)]. We can see that there is a lot of low frequency information in the envelopes, which is not the case for the original traces. Because of this property, we can fit the envelope rather than the original data in the misfit function so that the rich low frequency information can be used in the inversion.

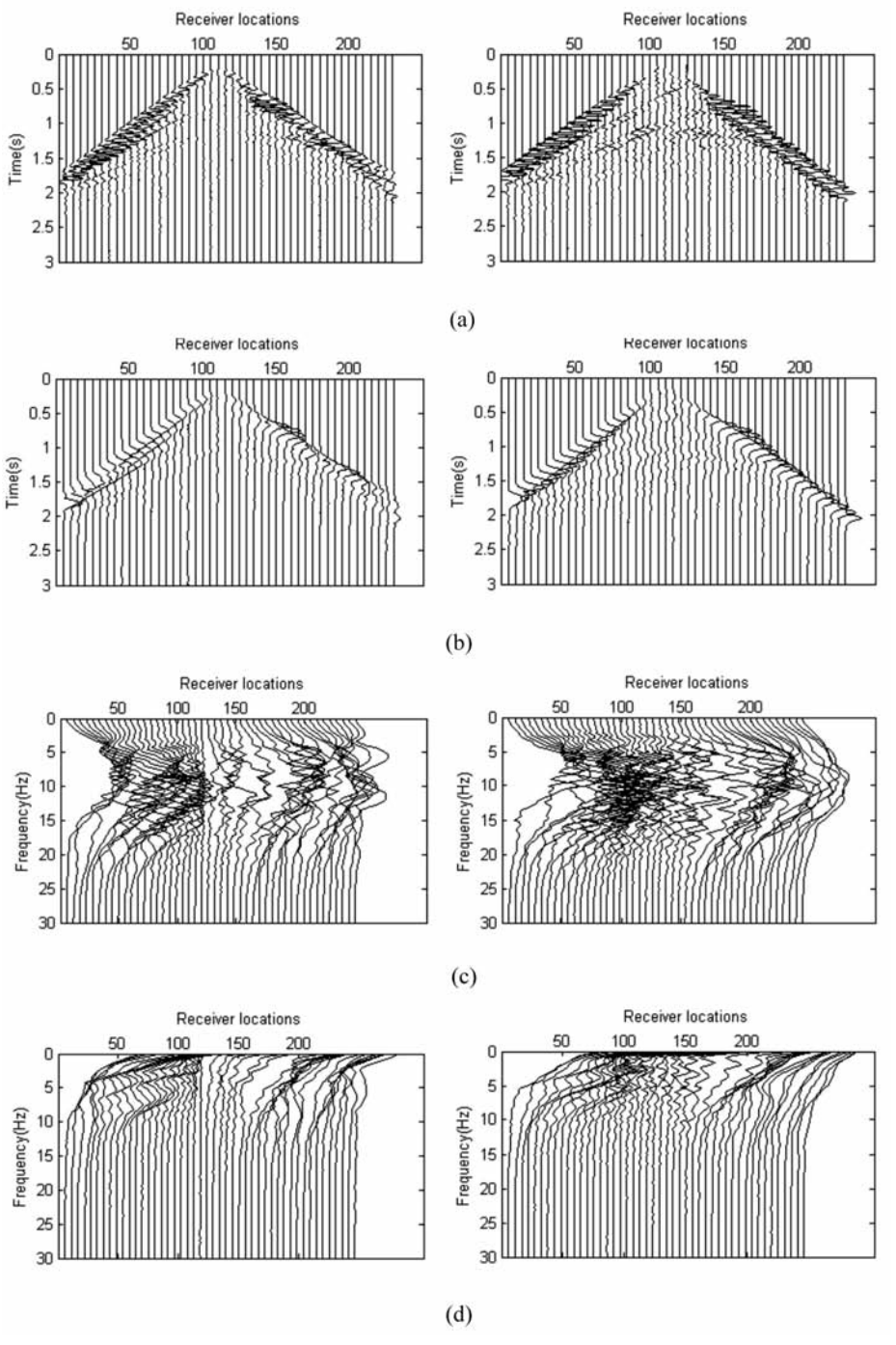

Fig. 1. (a) Data traces from the Marmousi II model; (b) trace envelope; (c) trace spectra; (d) envelope spectra. The left panels are for the x component and the right panels are for the z component.

Misfit function

As in our acoustic envelope inversion (Wu et al., 2013, 2014), the misfit function for the elastic envelope inversion can be defined as follows,

$$\sigma(\mathbf{m}) = \tfrac{1}{4} \sum_{sr} \sum_{i} \int_0^T |\{[e^i_{syn}(t)]^2 - e^i_{obs}(t)]^2\}|^2 dt \quad , \tag{10}$$

where e^i_{syn} and e^i_{obs} are the envelope of the i-th component of the synthetic wavefield and the observed wavefield, respectively, and $\mathbf{m}$ is the model parameter.

Using eq. (9), we can re-write eq. (10) into the following form,

$$\begin{aligned} \sigma(\mathbf{m}) &= \tfrac{1}{4} \sum_{sr} \sum_{i} \int_0^T |\{[s^i(t)]^2 + [s^i_H(t)]^2\} - \{[u^i(t) + [u^i_H(t)]^2\}|^2 dt \\ &= \tfrac{1}{4} \sum_{sr} \sum_{i} \int_0^T E_i^2 dt \quad , \end{aligned} \tag{11}$$

where s^i and u^i are the i-th component of the synthetic wavefield and the observed wavefield, respectively, s^i_H and u^i_H are the corresponding Hilbert transforms. E_i is the instant envelope data residual. In the above equation we applied a square to the envelope, because the squared envelope has better performance in large scale background recovery (Wu et al., 2013b; Luo et al., 2014).

Gradient calculation for elastic envelope inversion

In this paper, we assume the density is constant, and consider v_P and v_S as the model parameters. We calculate the derivative of the misfit function with respect to v_P and can get the following result,

$$\begin{aligned} \partial\sigma/\partial v_P &= \tfrac{1}{2} \sum_{sr} \sum_{i} \int_0^T E_i \left[\partial\{[s^i(t)]^2 + [s^i_H(t)]^2\}/\partial v_P\right] dt \\ &= \tfrac{1}{2} \sum_{sr} \sum_{i} \int_0^T E_i \left[2s^i(t)[\partial s^i(t)/\partial v_P] + 2s^i_H(t)[\partial s^i_H(t)/\partial v_P]\right] dt \end{aligned}$$

$$= \sum_{sr} \sum_{i} \int_{0}^{T} \left[E_i s^i(t) [\partial s^i(t)/\partial v_P] - H\{E_i s_H^i(t)\} [\partial s^i(t)/\partial v_P] \right] dt$$

$$= \sum_{sr} \sum_{i} \int_{0}^{T} [E_i s^i(t) - H\{E_i s_H^i(t)\}] [\partial s^i(t)/\partial v_P] dt \quad . \qquad (12)$$

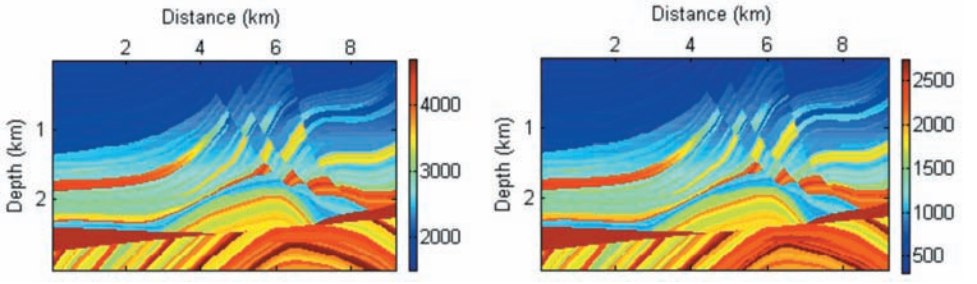

Fig. 2. The Marmousi II model. (a) P-wave velocity model; (b) S-wave velocity model.

Inversion with full frequency band source wavelet

We first show the validity of this method using a full frequency band source wavelet. The source wavelet is the Ricker wavelet with the dominant frequency of 10 Hz (Fig. 3).

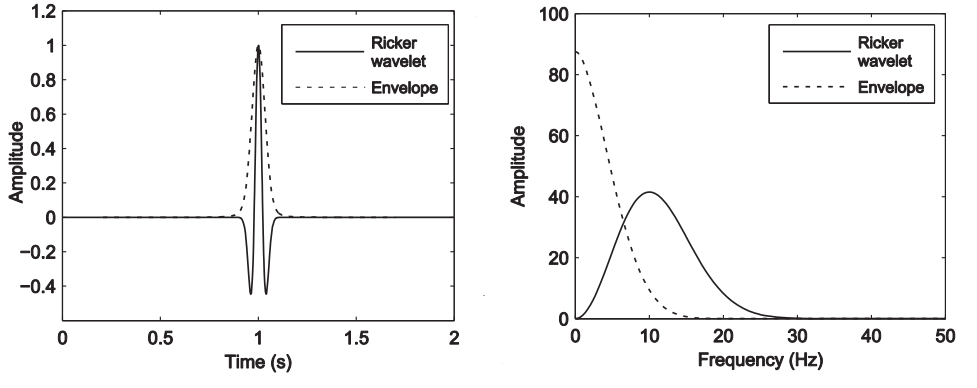

Fig. 3. (a) Time domain and (b) frequency domain full frequency band Ricker wavelet and its envelope.

We use the 1D linear initial model as the starting model (Fig. 4) and invert the P-wave velocity and S-wave velocity using elastic envelope inversion. Fig. 5 shows the envelope inversion results.

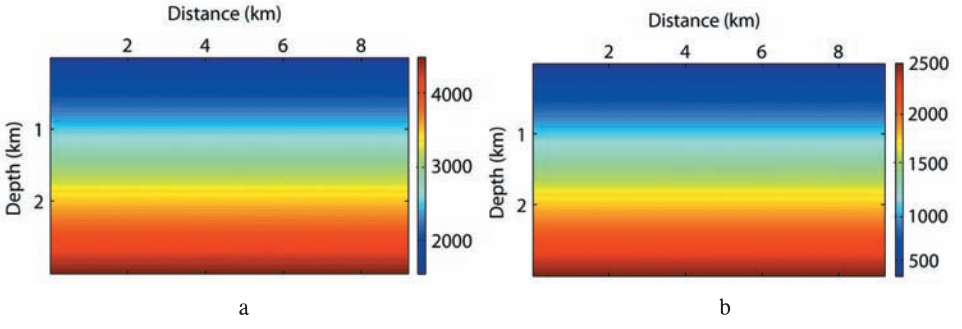

a b

Fig. 4. Linear initial model. (a) P-wave velocity model; (b) S-wave velocity model.

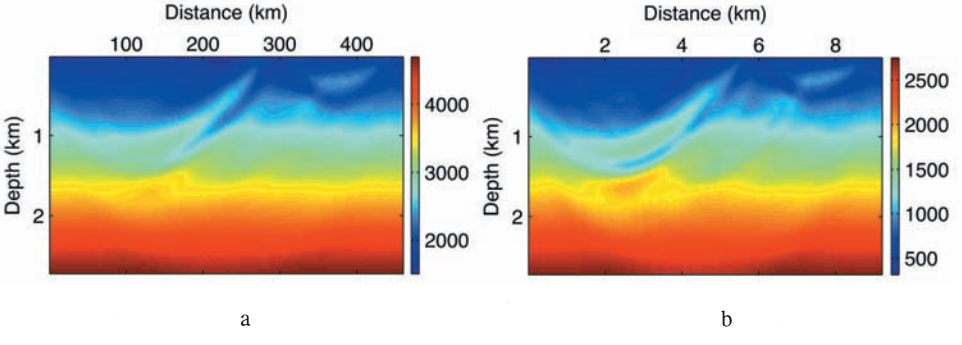

a b

Fig. 5. Envelope inversion results. (a) P-wave velocity model; (b) S-wave velocity model.

From these results we can already see the large scale component of the model which comes from the low frequency information in the data envelope. Based on these results, we can perform a successive elastic full waveform inversion using the results in Fig. 5 as the new initial model. Fig. 6 shows the final inversion results, which are the results from the combined elastic envelope inversion and waveform inversion. We can see that these results are very close to the true model. We also performed the conventional elastic full waveform inversion starting directly from the linear initial model and show the result in Fig. 7 as comparison. From the comparison we can easily see that the combined elastic envelope inversion and waveform inversion provides much better results than the conventional elastic full waveform inversion method.

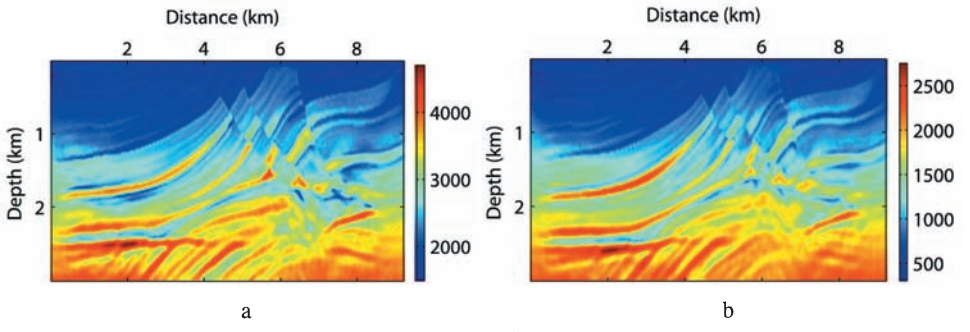

Fig. 6. Combined elastic envelope inversion and waveform inversion results. (a) P-wave velocity model; (b) S-wave velocity model.

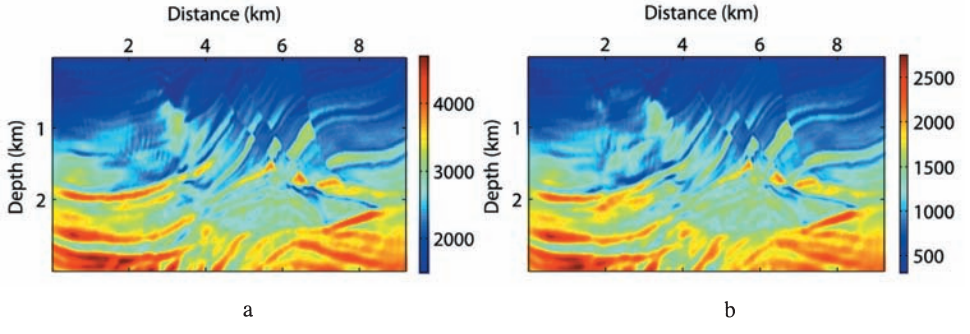

Fig. 7. Conventional elastic full waveform inversion results. (a) P-wave velocity model; (b) S-wave velocity model.

Inversion with the low cut source wavelet

To further demonstrate the ability of the elastic envelope inversion method, we perform the inversion using a low-cut source wavelet (with low frequencies below 5 Hz removed) as shown in Fig. 8. From the figure we can see that the low frequencies below 5 Hz has been removed from the source, however the envelope is still very rich in low frequency, which shows the independence of the low frequency in the envelope with the low frequency in the source wavelet.

We use this low-cut source to perform elastic envelope inversion and Fig.9 shows the envelope inversion results. If we compare these results with those in Fig. 5, we can see that although the results using low-cut source is not

as good as those using the full band source, however we can still clearly see the large-scale component in the results. As in the previous, we perform elastic full waveform inversion using the envelope inversion results as the new initial model. Fig. 10 shows the final combined elastic envelope inversion plus waveform inversion results. If we compare these results with those in Fig. 6, we can see that there is almost no difference in the final results. We also perform the conventional elastic full waveform inversion starting directly from the linear initial model and show the results in Fig. 11 as comparison. We can see that the conventional full waveform inversion results are influenced very much because of the lacking of low frequency information in the data and the results become even worse.

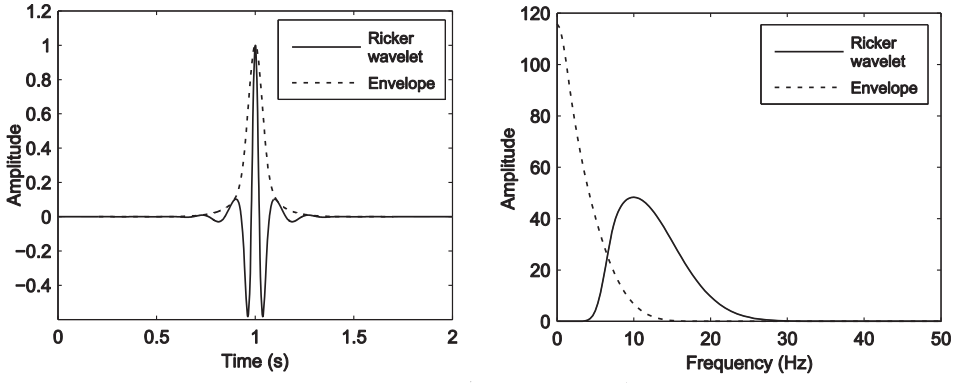

Fig. 8. (a) time domain and (b) frequency domain low-cut Ricker wavelet and its envelope.

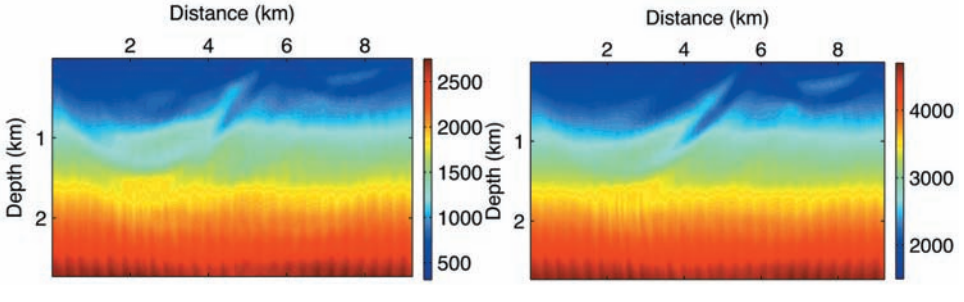

Fig. 9. Elastic envelope inversion results using the low-cut source. (a) P-wave velocity model; (b) S-wave velocity model.

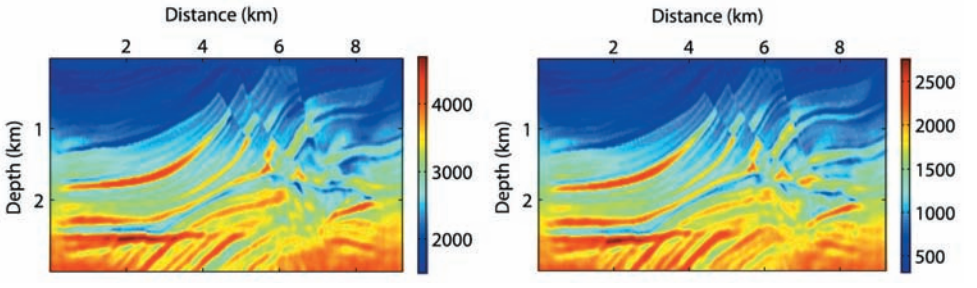

a b

Fig. 10. Combined elastic envelope inversion plus waveform inversion results using the low-cut source wavelet. (a) P-wave velocity model; (b) S-wave velocity model.

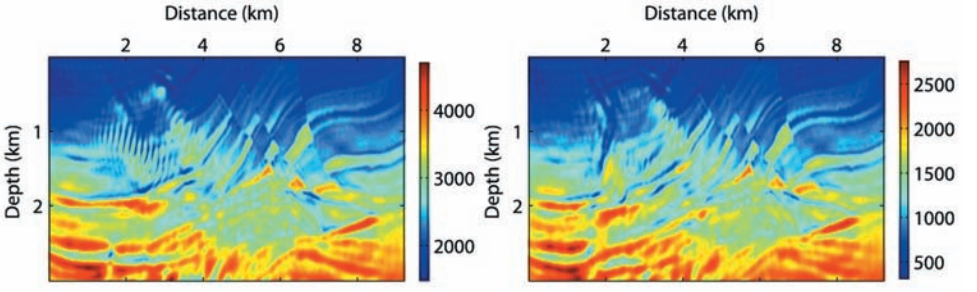

a b

Fig. 11. The conventional elastic full waveform inversion results using the low-cut source. (a) P-wave velocity model; (b) S-wave velocity model.

From the above tests we can see that the elastic envelope inversion method is very effective for the large-scale component model construction, even without low frequencies in the source wavelet.

CONCLUSION

In this paper, we extended our previously proposed acoustic envelope inversion method to the elastic situation. The data envelope is very rich in low frequency information, which can be used to retrieve the large scale component of the model. The gradient of P-wave velocity and S-wave velocity is obtained, and the validity of this method is proved by the numerical examples using the

Marmousi II model, where we used 1D linear initial model. The elastic envelope inversion is independent of the frequency band of the source wavelet. The P-wave velocity and S-wave velocity can be inverted effectively even without low frequencies in the source wavelet.

ACKNOWLEDGEMENTS

We thank Xiao-bi Xie for helpful discussions. This research is supported by the WTOPI Research Consortium at the University of California, Santa Cruz, USA.

REFERENCES

Biondi, B. and Almomin, A., 2012. Tomographic full waveform inversion (TFWI) by combining full waveform inversion with wave-equation migration velocity analysis. Expanded Abstr., 82nd Ann. Internat. SEG Mtg., Las Vegas: 1-5.

Biondi, B. and Almomin, A., 2013. Tomographic full waveform inversion (TFWI) by extending the velocity model along the time-lag axis. Expanded Abstr., 83rd Ann. Internat. SEG Mtg., Houston: 1031-1036.

Biondi, B. and Almomin, A., 2014. Efficient and robust waveform-inversion workflow: Tomographic FWI followed by FWI. Expanded Abstr., 84th Ann. Internat. SEG Mtg., Denver: 917-921.

Brenders, A.J. and Pratt, R.G., 2007. Full waveform tomography for lithospheric imaging: Results from a blind test in a realistic crustal model. Geophys. J. Internat., 168: 133-151.

Bunks, C., Saleck, F.M., Zaleski, S. and Chavent, G., 1995. Multiscale seismic waveform Inversion. Geophysics, 60: 1457-1473.

Crase, E., Wideman, C., Noble, M. and Tarantola, A., 1992. Nonlinear elastic waveform inversion of land seismic reflection data. J. Geophys. Res., 97: 4685-4703.

Debski, W. and Tarantola, A., 1995. Information of elastic parameters obtained from the amplitudes of reflected waves. Geophysics, 60: 1426-1436.

Djipéssé, H. and Tarantola, A., 1999. Multiparameters L_1 norm waveform fitting: Interpretation of Gulf of Mexico reflection seismograms. Geophysics, 64: 1023-1035.

Lailly, P., 1983. The seismic inverse problem as a sequence of before stack migration. Proc. SIAM Conf. Inverse Scatt.: Theory and Applications. Soc. Industr. Appl. Mathemat., Robinson, E. and Weglein, A. (Eds.), Philadelphia: 206-220.

Liu, J., Chauris, H. and Calandra, H., 2011. The normalized integration method - an alternative to full waveform inversion? Near Surface 2011, 17th EEEG Mtg., Leicester: B07.

Luo, J. and Wu, R.S., 2013. Envelope inversion - some application issues. Expanded Abstr., 83rd Ann. Internat. SEG Mtg., Houston: 1042-1047.

Luo, J. and Wu, R.S., 2014. Seismic envelope inversion: reduction of local minima and noise resistance. Geophys. Prosp., 63: 597-614.

Mora, P., 1987. Nonlinear two-dimensional elastic inversion of multi-offset seismic data. Geophysics, 52: 1211-1228.

Mora, P., 1988. Elastic wave-field inversion of reflection and transmission data. Geophysics, 53: 750-759.

Pratt, R.G., 1999. Seismic waveform inversion in the frequency domain, Part 1: Theory and verification in a physical scale model. Geophysics, 64: 888-901.

Pratt, R.G. and Shipp, R.M., 1999. Seismic waveform inversion in the frequency domain, Part 2: Fault delineation in sediments using crosshole data. Geophysics, 64: 902-914.

Sambridge, M.S., Tarantola, A. and Kennett, B.L.N., 1991. An alternative strategy for non-linear inversion of seismic waveforms. Geophys. Prosp., 39: 723-736.
Sears, T.J., Singh, S.C. and Barton, P.J., 2008. Elastic full waveform inversion of multi-component OBC seismic data. Geophys. Prosp., 56: 843-862.
Sears, T.J., Barton, P.J. and Singh, S.C., 2010. Elastic full waveform inversion of multicomponent ocean-bottom cable seismic data: Application to Alba Field, U.K. North Sea. Geophysics, 75: R109-R119.
Shin, C. and Cha, Y.H., 2008. Waveform inversion in the Laplace domain. Geophys. J. Int., 173: 922-931.
Shin, C. and Cha, Y.H., 2009. Waveform inversion in the Laplace-Fourier domain. Geophys. J. Int., 177: 1067-1079.
Tarantola, A., 1984. Inversion of seismic reflection data in the acoustic approximation. Geophysics, 49: 1259-1266.
Tarantola, A., 1986. A strategy for nonlinear elastic inversion of seismic reflection data. Geophysics, 51: 1893-1903.
Wang, H., Singh, S.C., Jian, H. and Calandra, H., 2012. Integrated inversion of subsurface velocity structures using wave equation tomography and full waveform inversion. Expanded Abstr, 82nd Ann. Internat. SEG Mtg., Las Vegas: 1-5.
Warner, M. and Guasch, L., 2014. Adaptive waveform inversion: Theory. Expanded Abstr., 84th Ann. Internat. SEG Mtg., Denver: 1089-1093.
Wu, R.S., Luo, J. and Wu, B., 2013. Ultra-low-frequency information in seismic data and envelope inversion. Expanded Abstr., 83rd Ann. Internat. SEG Mtg., Houston: 3078-3082.
Wu, R.S., Luo, J. and Wu, B., 2014. Seismic envelope inversion and modulation signal model. Geophysics, 79: WA13-WA24.

APPENDIX A

GRADIENT CALCULATION FOR ELASTIC FULL WAVEFORM INVERSION

We first calculate the gradient of the misfit function with respect to λ and η. The gradient with respect to v_P and v_S can be obtained by eq. (2).

First we define the gradient of the wavefield u^i with respect to λ and η as

$$\begin{aligned} \mathbf{J}^i_\lambda &= U^i_\lambda(r_g,t;r) = \partial u^i(r_g,t)/\partial\lambda(r) \quad , \\ \mathbf{J}^i_\mu &= U^i_\mu(r_g,t;r) = \partial u^i(r_g,t)/\partial\mu(r) \quad , \end{aligned} \tag{A-1}$$

where r_g is the receiver location.

We assume a small perturbation in the model space $\delta\lambda$ and $\delta\eta$, which caused a small perturbation to the wavefield, then we have

$$\begin{cases} \rho(\partial^2 u^i/\partial t^2) - (\partial \tau^{ij}/\partial x^j) = f^i \\ \tau^{ij} = M^{ij} + \lambda\delta^{ij}u_{k,k} + \mu(u_{i,j} + u_{j,i}) \end{cases} . \tag{A-2}$$

$$\begin{cases} \rho[\partial^2(u + \delta u)^i/\partial t^2] - [\partial(\tau + \delta\tau)^{i\,j}/\partial x^j]) = f^i \\ (\tau+\delta\tau)^{i\,j} = M^{i\,j} + (\lambda+\lambda\delta)\delta^{i\,j}(u+\delta u)_{k,k} + (\mu+\delta\mu)[(u+\delta u)_{i,j} + [(u+\delta u)_{j,i}] \end{cases} \quad (A\text{-}3)$$

Subtract (A-3) by (A-2), we have

$$\begin{aligned} &\rho(\partial^2\delta u^i/\partial t^2) - (\partial\delta\tau^{i\,j}/\partial x^j) = 0 \\ &\delta\tau^{i\,j} = \delta\lambda\delta^{i\,j}u_{k,k} + \delta\mu(u_{i,j} + u_{j,i}) + \lambda\delta^{i\,j}\delta u_{k,k} + \mu(\delta u_{i,j} + \delta u_{j,i}) \end{aligned} \quad (A\text{-}4)$$

From the analytic solution of the elastic wave equation, we know that,

$$\begin{aligned} \delta u^i(r,t) &= -\int_V dV(r') \int dt'[\partial G^{i\,j}(r,t;r',t')/\partial x^k]\delta M^{jk}(r',t') \\ &= -\int_V dV(r') \int dt'[\partial G^{i\,j}(r,t;r',t')/\partial x^k] \\ &\quad \times [\delta\lambda(r')\delta^{jk}u_{l,l} + \delta\mu(r')(u_{j,k} + u_{k,j})] \\ &= -\int_V dV(r') \int dt'[\partial G^{i\,j}(r,t;r',t')/\partial x^k] \\ &\quad \times [\delta^{jk}u_{l,l}\cdot\delta\lambda(r') - \int_V dV(r') \int dt'[\partial G^{i\,j}(r,t;r',t')/\partial x^k] \\ &\quad \times (u_{j,k} + u_{k,j})\cdot\delta\mu(r') \quad . \end{aligned} \quad (A\text{-}5)$$

From the above equation we can get,

$$\begin{aligned} U^i_\lambda(r_g,t;r) &= -\int dt'[\partial G^{i\,j}(r_g,t;r,t')/\partial x^k]\delta^{jk}u_{l,l} \quad , \\ U^i_\mu(r_g,t;r) &= -\int dt'[\partial G^{i\,j}(r_g,t;r,t')/\partial x^k](u_{j,k} + u_{k,j}) \quad . \end{aligned} \quad (A\text{-}6)$$

From the definition of the misfit function in eq. (3), we can get similar results as that in eq. (6) for λ and η,

$$\begin{aligned} \partial\sigma/\partial\lambda &= \mathbf{J}^T_\lambda\boldsymbol{\eta} \\ \partial\sigma/\partial\mu &= \mathbf{J}^T_\mu\boldsymbol{\eta} \end{aligned} \quad (A\text{-}7)$$

Substitute eq. (A-6) into (A-7), and we get

$$\partial\sigma/\partial\lambda = -\sum_g \int dt \int dt'[\partial G^{i\,j}(r_g,t;r,t')/\partial x^k]\delta^{jk}u_{l,l}\delta u^i(r_g,t)$$

$$= -\int dt' \sum_g \int dt[\partial G^{i\,j}(r_g,t;r,t')/\partial x^j]\delta u^i(r_g,t)u_{l,l}$$

$$= -\int dt' u_{l,l}\overleftarrow{u}_{j,j} \quad , \tag{A-8}$$

$$\partial\sigma/\partial\mu = -\sum_g \int dt \int dt'[\partial G^{i\,j}(r_g,t;r,t')/\partial x^k](u_{j,k} + u_{k,j})\delta u^i(r_g,t)$$

$$= -\int dt' \sum_g \int dt[\partial G^{i\,j}(r_g,t;r,t')/\partial x^j]\delta u^i(r_g,t)(u_{j,k} + u_{k,j})$$

$$= -\int dt'(u_{j,k} + u_{k,j})\overleftarrow{u}_{j,k} \quad , \tag{A-9}$$

where "$\leftarrow$" means backpropagation wavefields.

From eq. (2) we can get the gradient of the misfit function with respect to v_P and v_S as follows

$$\partial\sigma/\partial v_P = -2\rho v_P \int dt\, u_{l,l}\overleftarrow{u}_{j,j} \quad , \tag{A-10}$$

$$\partial\sigma/\partial v_S = -4\rho v_S \int dt\, u_{l,l}\overleftarrow{u}_{j,j} - 2\rho v_S \int dt\,(u_{j,k} + u_{k,j})\overleftarrow{u}_{j,k} \quad . \tag{A-11}$$

APPENDIX B

GRADIENT CALCULATION FOR ELASTIC ENVELOPE INVERSION

From the definition of the misfit function in eq. (10), we can get similar results as that in eq. (15) for λ and η,

$$\begin{aligned} \partial\sigma/\partial\lambda &= \mathbf{J}_\lambda^T\boldsymbol{\eta} \\ \partial\sigma/\partial\mu &= \mathbf{J}_\mu^T\boldsymbol{\eta} \end{aligned} \quad . \tag{B-1}$$

where

$$\begin{cases} \mathbf{J}_\lambda = \partial u^i/v_\lambda \\ \mathbf{J}_\mu = \partial u^i/v_\mu \end{cases} \quad , \quad \boldsymbol{\eta} = E_i u^i(t) - H\{E_i u_H^i(t)\} \quad . \tag{B-2}$$

Substitute eqs. (A-6) and (B-2) into (B-1), we get

$$\begin{aligned}\partial\sigma/\partial\lambda &= -\sum_g \int dt \int dt'[\partial G^{i,j}(r_g,t;r,t')/\partial x^k]\delta^{jk}u_{l,l} \\ &\quad \times [E_i u^i(t) - H\{E_i u_H^i(t)\}](r_g,t) \\ &= -\int dt' \sum_g \int dt[\partial G^{i,j}(r_g,t;r,t')/\partial x^j][E_i u^i(t) - H\{E_i u_H^i(t)\}]u_{l,l} \\ &= -\int dt' u_{l,l}\overleftarrow{\tilde{u}}_{j,j} \quad , \end{aligned} \tag{B-3}$$

$$\begin{aligned}\partial\sigma/\partial\mu &= -\sum_g \int dt \int dt'[\partial G^{i,j}(r_g,t;r,t')/\partial x^k](u_{j,k} + u_{k,j}) \\ &\quad \times [E_i u^i(t) - H\{E_i u_H^i(t)\}](r_g,t) \\ &= -\int dt' \sum_g \int dt[\partial G^{i,j}(r_g,t;r,t')/\partial x^k] \\ &\quad \times [E_i u^i(t) - H\{E_i u_H^i(t)\}](r_g,t)(u_{j,k} + u_{k,j}) \\ &= -\int dt'(u_{j,k} + u_{k,j})\overleftarrow{\tilde{u}}_{j,k} \quad , \end{aligned} \tag{B-4}$$

where "$\leftarrow$" means backpropagation wavefields and "$\tilde{}$" means this backpropagation wavefields is obtained by using envelope residual.

From eq. (2) we can get the gradient of the misfit function with respect to v_P and v_S as follows

$$\partial\sigma/\partial v_P = -2\rho v_P \int dt\, u_{l,l}\overleftarrow{\tilde{u}}_{j,j} \quad , \tag{B-5}$$

$$\partial\sigma/\partial v_S = -4\rho v_S \int dt\, u_{l,l}\overleftarrow{\tilde{u}}_{j,j} - 2\rho v_S \int dt\,(u_{j,k} + u_{k,j})\overleftarrow{\tilde{u}}_{j,k} \quad . \tag{B-6}$$